Surface & Coatings Technology 205 (2010) 245–250

Contents lists available at ScienceDirect

Surface & Coatings Technology

journal homepage: www.elsevier.com/locate/surfcoat

Microstructure and wear characteristics of hypereutectic Fe–Cr–C cladding with various carbon contents

Chia-Ming Chang [a], Li-Hsien Chen [a], Chi-Ming Lin [a], Jie-Hao Chen [a], Chih-Ming Fan [b], Weite Wu [a,*]

[a] Department of Materials Science and Engineering, National Chung Hsing University, 250 Kuo-Kuang Rd., Taichung, Taiwan
[b] Kuang Tai Metal Industrial Co., Ltd.,8 Lu-Ke Third Rd., Lujhu Township, Kaohsiung, Taiwan

ARTICLE INFO

Article history:
Received 31 August 2009
Accepted in revised form 9 June 2010
Available online 23 June 2010

Keywords:
Hardfacing
Welding
Chromium carbide
Abrasive wear

ABSTRACT

The current study used flux core arc welding to produce a series of hypereutectic Fe–Cr–C claddings with various carbon content. Depending on the carbon content, this research produced hypereutectic microstructures of γ-Fe + $(Cr,Fe)_7C_3$ carbides. As the carbon content of a cladding increased from 3.73 to 4.85 wt.%, the surface fractions of carbides increased from 33.8% to 86.1%. The morphology of primary $(Cr,Fe)_7C_3$ carbides also transited from a blade-like to a rod-like shape. With regard to wear performance, the relationship between wear resistance and hardness (H) is non-linear. However, the mean free path (λ) of primary $(Cr,Fe)_7C_3$ carbides must be considered. Wear resistance is proportional to H/λ. The primary carbides can prevent the eutectic colonies from selective abrasion. The rod-like $(Cr,Fe)_7C_3$ carbides also provide much better wear resistance because rod-like carbides have a greater hardness. After an abrasive wear process, abrasive particles cause plastic plows when the cladding has lower surface fractions of carbides. The fracture of primary carbides leads into the craters where it occurs in the worn cladding surface with higher surface fractions of carbides.

1. Introduction

Hardfacing materials in severe abrasive conditions widely use Fe–Cr–C alloys due to their superior abrasion resistance. Excellent abrasive wear resistance results from a high volume of carbides and matrix toughness [1]. Properties, such as abrasion wear resistance, surface roughening resistance and seizing or sticking resistance, are essential for these alloyed white cast irons used for rolls and other wear-resistant parts in steel rolling and mineral pulverizing mills. Among these properties, abrasion wear resistance is reportedly dependent not only on type, morphology, amount and the distribution pattern of the carbides precipitated from the melt, but also on the type of matrix structure [2].

Proeutectic $(Cr,Fe)_7C_3$ carbides are found in Fe–Cr–C alloys with a high carbon content (2–5 wt.%) and a high chromium content (18–30 wt.%). Such microstructures have good wear resistance properties. These hard materials can be represented by high chromium white cast iron (M_7C_3), which has high hardness (about 1600 Hv) [3–6]. Cr_7C_3 is well known for its excellent combination of high hardness and excellent wear resistance as well as good corrosion and oxidation resistance. Most hard composite coatings have widely used Cr_7C_3 as the reinforcing phase [7–10]. The proeutectic $(Cr,Fe)_7C_3$ carbides with high hardness successfully retard plastic deformation when interacting with the counter surface during the sliding wear process. Therefore, the effect of adhesive deformation on material removal rate is low. The coarser proeutectic $(Cr,Fe)_7C_3$ carbides play a dominant wear-resisting role in the dry sliding wear process. With the protection of the hard and wear-resistant primary $(Cr,Fe)_7C_3$ carbides, the $(Cr,Fe)_7C_3$/γ-Fe eutectic matrix avoids severe selective wear. Primary $(Cr,Fe)_7C_3$ carbides are also supported by the fine, strong and ductile $(Cr,Fe)_7C_3$/γ-Fe eutectic matrix. During the dry sliding wear process, with the support of the $(Cr,Fe)_7C_3$/γ-Fe eutectic matrix, the coarse primary $(Cr,Fe)_7C_3$ phases avoid spalling and delamination [11].

This study investigated the relationship between wear resistance and the microstructure of hypereutectic Fe–Cr–C cladding, and discusses the interaction among primary carbides, eutectic colonies and abrasive particles. Combining wear resistance and worn surface observations, this study found the wear mechanism of hypereutectic Fe–Cr–C cladding to provide information for selecting hypereutectic Fe–Cr–C cladding.

2. Experiment procedures

The base metals for the welding surface were prepared from ASTM A36 steel plates (100 mm × 80 mm × 10 mm). Before welding, these specimens were ground and cleaned with acetone. To obtain the hypereutectic Fe–Cr–C claddings with various carbon contents, the chemical compositions of all hypereutectic claddings lay within the M_7C_3 phase field. The different amounts of graphite (7, 10 and 13 wt.%), the constant chromium powder (40 wt.%), and ferrosilicon (2 wt.%), ferromanganese (5 wt.%), iron powder (46, 43 and 40 wt.%) were added into flux cored wire with a 2.8 mm diameter. The addition of ferrosilicon and ferromanganese was used to reduce the oxygen of the claddings.

* Corresponding author. Tel.: +886 4 22879000; fax: +886 4 22857017.
E-mail address: wwu@nchu.edu.tw (W. Wu).

0257-8972/$ – see front matter © 2010 Elsevier B.V. All rights reserved.
doi:10.1016/j.surfcoat.2010.06.021

Table 1
Chemical compositions and surface fractions of carbides of hypereutectic cladding and base metal.

Cladding	Composition (wt.%)					Surface fractions of carbides (%)
	C	Si	Mn	Cr	Fe	
Base metal	0.18 ± 0.03	0.15 ± 0.02	0.55 ± 0.03	0.09 ± 0.02	Bal.	–
A	3.73 ± 0.05	2.28 ± 0.07	2.33 ± 0.05	26.70 ± 0.08	Bal.	33.81 ± 2.3
B	4.21 ± 0.03	2.00 ± 0.05	2.26 ± 0.06	27.08 ± 0.09	Bal.	61.19 ± 3.1
C	4.85 ± 0.02	1.96 ± 0.05	2.28 ± 0.05	27.31 ± 0.09	Bal.	86.14 ± 2.7

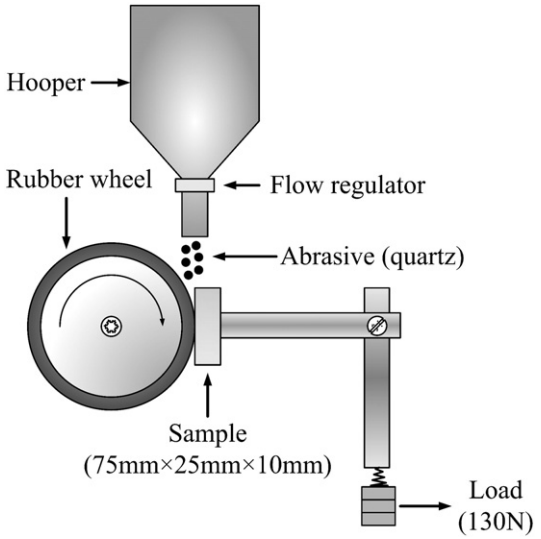

Fig. 1. Schematic of the dry sand–rubber wheel testing machine.

Bead-on-plate with oscillate flux cored arc welding was utilized to deposit the hypereutectic Fe–Cr–C claddings. The welding current and voltage were 350 A and 33 V. The welding speed was 200 mm/min and the distance from contact tube to work was 50 mm. The thickness of all claddings was about 5 mm. The experiment utilized an optical emission spectrograph (OES) to analyze chemical composition of the claddings. Table 1 shows the chemical composition of claddings and base metal.

X-ray diffraction (XRD) specimens were prepared from the top surface of the hardfacing, and X-ray diffraction with Cu Kα radiation analyzed the constituent phases. The cladding structures were examined by optical microscopy (OM). Microstructure investigations were carried out on the top surface of the claddings after polishing and etching. The etching agent was composed of 20 g ammonium hydrogen fluoride, 0.5 g potassium pyrosulfite, and 100 ml H_2O at 80 °C. This study used image analysis software to analyze quantitatively the surface fractions of carbides. Ten pictures at 50 magnifications were taken for quantitative surface fractions of carbides. Quantitative elemental analysis of constituent phases was performed by a wavelength dispersive X-ray spectrometer (WDS).

The hardness of constituent phases in the microstructure was measured by a microhardness tester with 0.98 N load. Abrasive wear tests were carried out in a dry sand–rubber wheel testing machine (Fig. 1) according to ASTM G65 standards. Rounded quartz particles with a mean diameter between 200 and 300 μm were used, with a hardness of 1000–1100 Hv. After the wear test, the worn surface was examined by optical microscope and scanning electron microscope.

3. Results and discussion

The current study used flux cored arc welding to produce claddings containing different carbon contents on ASTM A36 steel substrates. Fig. 2 shows a liquidus projection of the iron corner of the Fe–Cr–C ternary system [12–14], with points A, B and C corresponding to the claddings listed in Table 1. The chemical compositions of all hypereutectic claddings lie within the M_7C_3 phase field. Therefore, the primary $(Cr,Fe)_7C_3$ carbides precipitate first when the melt pool begins to solidify.

Fig. 3 presents the phases of hardfacing alloys with different carbon contents produced by flux cored arc welding process. The XRD results indicate that the austenite (γ) with f.c.c structure and $(Cr,Fe)_7C_3$ with hexagonal structure occur in all claddings. Furthermore, the microstructures obtained for all cladding, as presented in Fig. 4, are composed of the blade-like, rod-like carbides and eutectic colonies. The chemical compositions and Cr/Fe atomic ratios of the individual phases presented

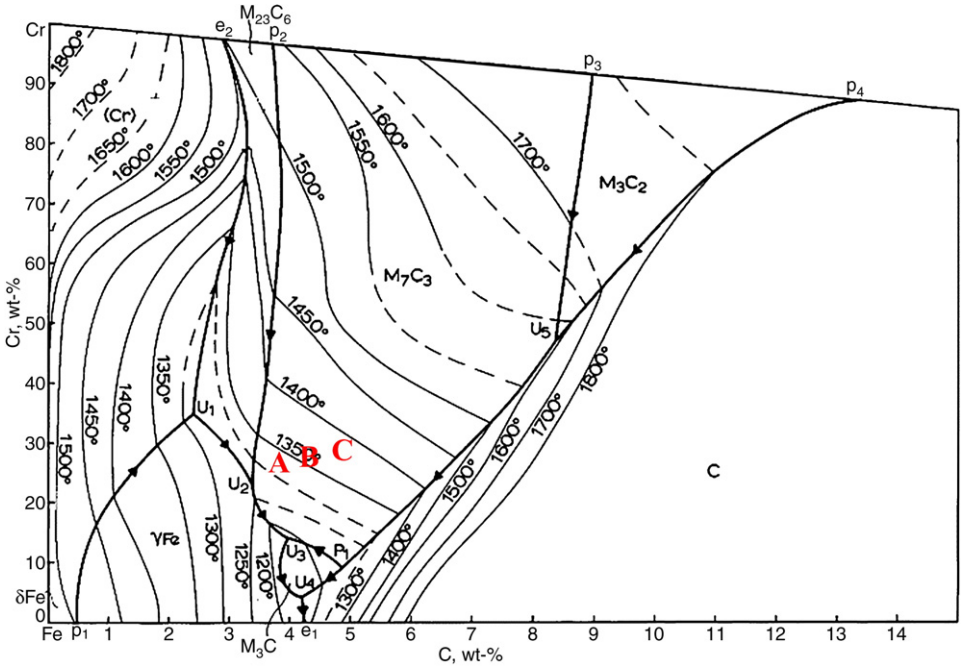

Fig. 2. Liquidus projection of the iron corner of the Fe–Cr–C ternary system [12–14].

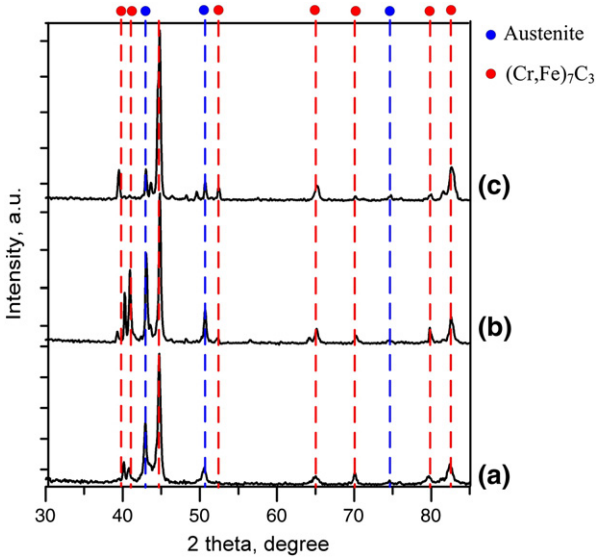

Fig. 3. X-ray spectrums of claddings with different carbon contents: (a) 3.73 wt.% C; (b) 4.21 wt.% C; and (c) 4.85 wt.% C.

in the microstructure of high chromium Fe–Cr–C hardfacing alloys are analyzed by electron probe microanalysis (Table 2). This quantitative elemental analysis confirms that the primary carbide in cladding is $(Cr,Fe)_7C_3$ carbide. The Cr/Fe ratios of $(Cr,Fe)_7C_3$ carbides with different shape are 1.31 and 1.29, respectively. The chemical composition of blade-like carbides is similar to that of rod-like ones. For the eutectic colonies, the atomic ratio of Cr/Fe is approximately 0.14. Comparing the previous study [15], for Fe–40 wt.% Cr–C cladding, the Cr/Fe ratios of M_7C_3 and eutectic colonies are 3.10 and 0.78, respectively. Therefore, the cladding with high chromium content causes high Cr/Fe ratios.

Previous research [16–19] reports that primary M_7C_3 carbides are classified by two morphologies, including rod-like and blade-like shapes in Fe–Cr–C systems. In Fig. 3, the morphology of primary $(Cr,Fe)_7C_3$ carbide transitions from blade-like to rod-like depending on the carbon content of cladding. The solidification morphology and the growth pattern of the cladding metal are controlled by weld pool thermal conditions. The formation and growth of primary $(Cr,Fe)_7C_3$ carbides during solidification occur with their long axes parallel to the direction of the heat flow. When carbon content is lower, the nuclei sites of primary $(Cr,Fe)_7C_3$ carbides are fewer and their growth direction is random. The primary $(Cr,Fe)_7C_3$ carbide rods appear as blade-like shapes when their axis are perpendicular to the viewing surface. With increasing carbon content of claddings, the nuclei sites of primary $(Cr,Fe)_7C_3$ carbides

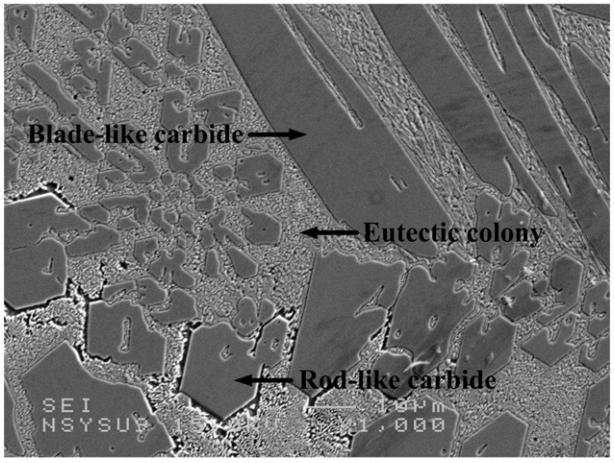

Fig. 4. SEM photograph of hypereutectic Fe–Cr–C cladding.

Table 2
Chemical compositions of each phase by WDS.

Phase	C	Cr	Fe	Cr/Fe ratio
Blade-like carbide	8.91 wt.% (30.4 at.%)	51.59 wt.% (40.7 at.%)	39.50 wt.% (28.9 at.%)	1.31 (1.41)
Rod-like carbide	8.83 wt.% (30.2 at.%)	51.44 wt.% (40.6 at.%)	39.73 wt.% (29.2 at.%)	1.29 (1.39)
Eutectic colony	3.70 wt.% (15.1 at.%)	11.52 wt.% (10.8 at.%)	84.78 wt.% (74.1 at.%)	0.14 (0.15)

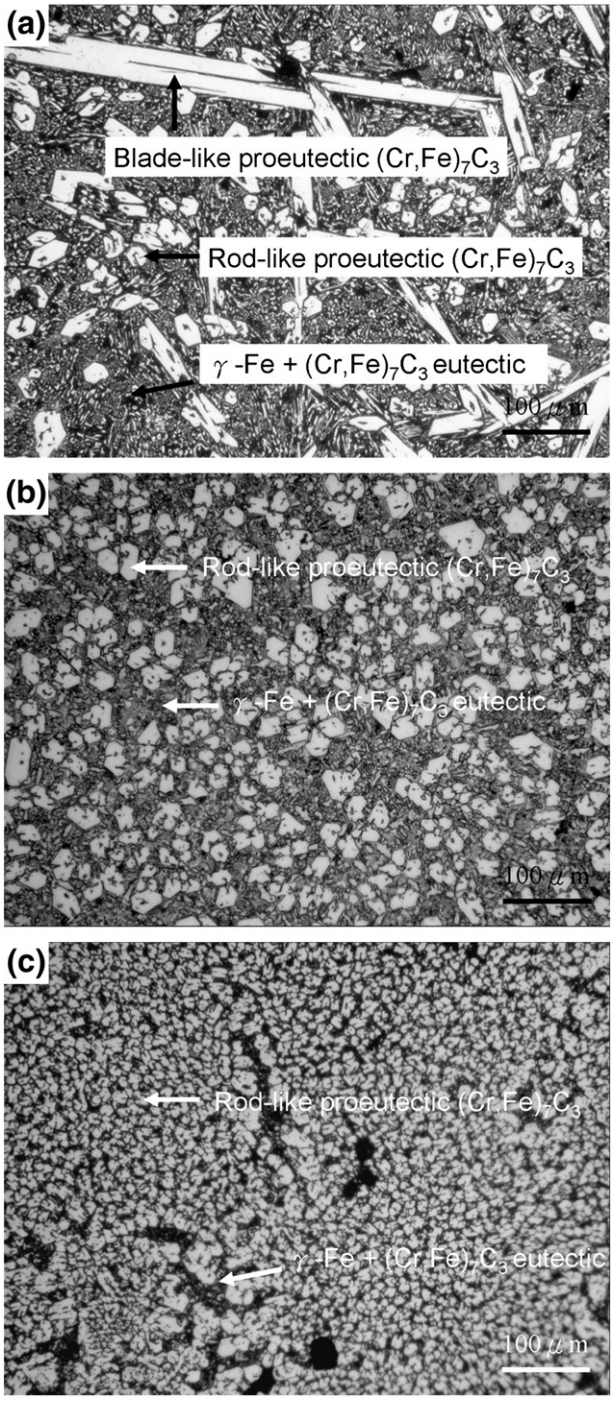

Fig. 5. Microstructure of claddings with different carbon contents: (a) 3.73 wt.% C; (b) 4.21 wt.% C; and (c) 4.85 wt.% C.

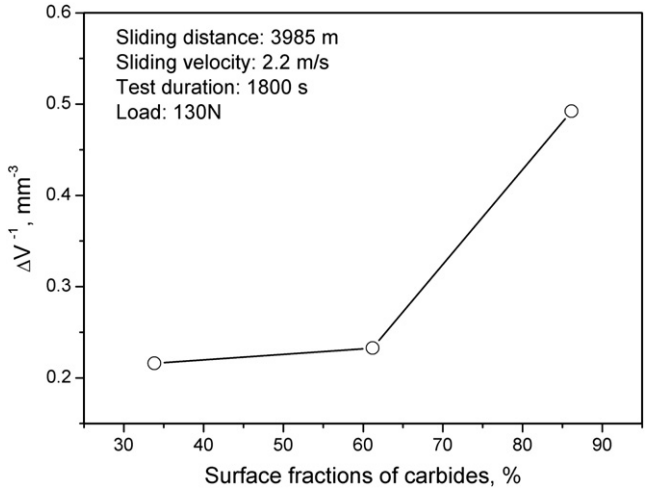

Fig. 6. Effect of surface fractions of carbides on the wear resistance of cladding.

increase. The $(Cr,Fe)_7C_3$ carbide rods appear as blade-like shapes when their axis are perpendicular to the viewing surface. The morphology of primary $(Cr,Fe)_7C_3$ carbides transits from blade-like to rod-like as the carbon content of claddings increases.

With the temperature decreasing, the eutectic colonies appear around the primary $(Cr,Fe)_7C_3$ grain boundary, as shown in Fig. 5. Therefore, these claddings have a hypereutectic structure containing primary $(Cr,Fe)_7C_3$ and eutectic colonies of austenite plus $(Cr,Fe)_7C_3$. Moreover, the surface fractions of carbides increased from 33.8 to 86.1% with the carbon content increasing from 3.73 to 4.85 wt.%. For an off-eutectic composition, the alloy liquidus is much higher than the eutectic temperature. Thus the corresponding primary phase which has higher undercooling tends to grow faster than the eutectic [20]. Comparing Fig. 5 a, b and c indicates that increasing the carbon content promotes the formation of primary $(Cr,Fe)_7C_3$ carbide. The carbon addition lowered the eutectic temperature for the Fe–Cr–C alloy [21]. The lower eutectic temperature results in less eutectic colonies. Consequently, the addition of carbon content promotes the formation of primary $(Cr,Fe)_7C_3$ carbides, but suppresses the growth of eutectic colonies.

Wear resistance is dependent on morphology, size, amount and distribution of carbides. R. Colaço suggested the following mathematical model [22]:

$$Q = K\frac{F_N}{H_0 + \beta x} + x\psi, \quad (1)$$

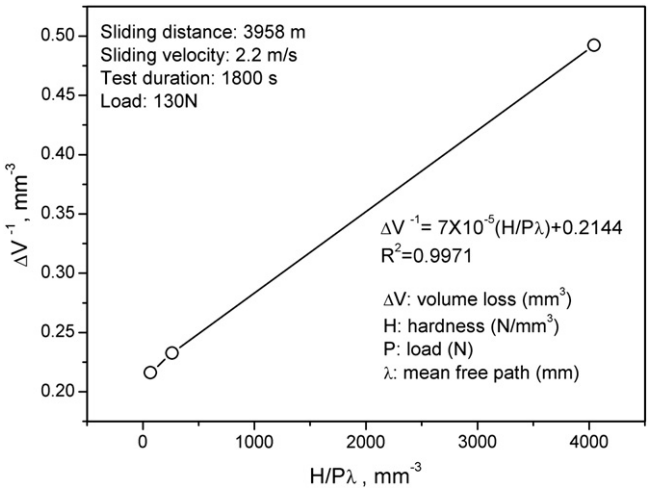

Fig. 7. Plot of wear resistance against H/λ.

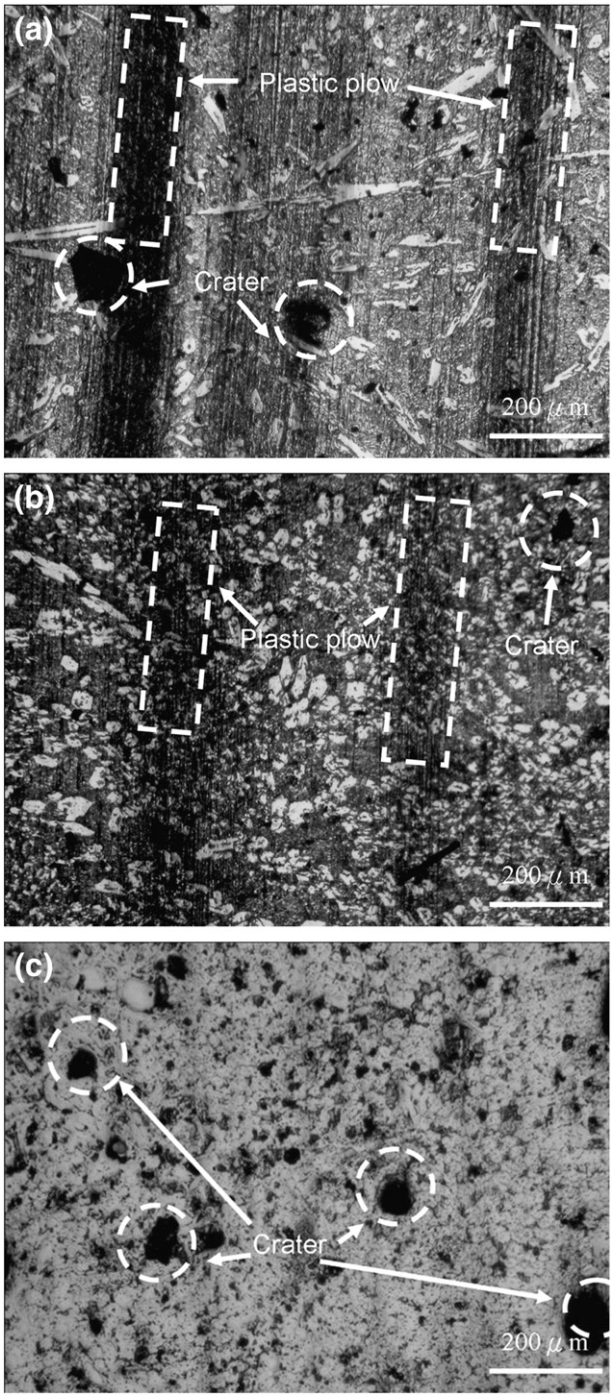

Fig. 8. Marco-observation for worn surface of claddings containing different carbon contents: (a) 3.73 wt.% C; (b) 4.21 wt.% C; and (c) 4.85 wt.% C.

Table 3
Microhardness of primary $(Cr,Fe)_7C_3$ carbides and the eutectic colony.

Cladding	Hardness (HV)		
	Primary $(Cr,Fe)_7C_3$ carbides		Eutectic colony
	Blade-like	Rod-like	
A	1109 ± 21	1324 ± 26	794 ± 36
B	–	1325 ± 17	792 ± 27
C	–	1371 ± 13	797 ± 31

where Q is wear rate, K is wear constant, F_N is the normal load applied to the abrasive particle, H_0 is material hardness, x is the volume fraction of reinforcement particles and β and ψ are constants, respectively.

Fig. 6 shows the relationship between the surface fractions of carbides and wear resistance. This result indicates that more surface fractions of carbides improve cladding wear resistance. This is because the elevated contents of hard primary $(Cr,Fe)_7C_3$ carbides provide a barrier against indentation, grooving and cutting of abrasive particles. The relationship between wear resistance and surface fractions of carbides is non-linear. Wear resistance rapidly accelerates as surface fractions of carbides increase. Therefore, wear resistance not only depends upon surface fractions of carbides and hardness. Abrasives must be small enough to fit between the carbide rods so that they sink deeper into the matrix and push the carbide from behind. If the abrasive is large compared to inter-carbide spacing, abrasive particles will slide over the carbides without significantly penetrating the matrix [23]. Thus, the mean free path of carbides also affects wear resistance. Fig. 7 illustrates the plot of wear resistance against H/λ, showing that the relation between wear resistance and H/λ is linear. The combination of hardness and mean free path is the main factor of wear resistance.

Wear mechanism typically classifies into four types of interactions between abrasive particles and a wearing material, namely microploughing, microcutting, microfatigue and microcracking. Microploughing due to a single pass of one abrasive particle does not result in any material detachment from the wearing surface. A prow forms ahead of the abrading particle and the material is continuously displaced sideways to form ridges adjacent to the groove produced. Pure microcutting results in a volume loss by chips equal to the volume of wear grooves. Microcracking occurs when abrasive particles impose on highly concentrated stresses, particularly on the surface of brittle materials. Microploughing and microcutting are the dominant processes for ductile materials while microcracking becomes important on brittle materials [24].

Fig. 8 shows the observation for worn surfaces of hypereutectic Fe–Cr–C claddings with various carbon contents. The plastic prows and craters appear in Fig. 8 (a) and (b). With surface fractions of carbides increasing, the plastic plows gradually disappear. Finally, no plastic prows appear in the worn surface of cladding with higher carbon content, as shown in Fig. 8 (c). The plastic plows arise from abrasive particles embedded into the rubber wheel surface and act as fixed indenters, causing the so-called grooving wear mode. Microplowing by the abrasive particles causes extensive matrix deformation, forming pile-ups along the groove edges. The grooves become narrower and shallower when the abrasive particles move across the carbides. The higher surface fractions of carbides lead to the disappearance of plastic plows. The craters also exist in the worn surface of each cladding. Crater formation is due to abrasive particles continuously attacking the carbides causing carbide fracture and pullout.

Wear behavior typically depends on the hardness ratio of abrasive particles and material. An abrasive particle is called “hard” if its hardness is about 20% greater than the hardness of the stressed material in a worn condition [25]. Hard abrasive particles easily dig out small phases and cut or crack larger ones. Soft abrasive particles are able to dig out small phases or produce large pits [24]. According to Zum Gahr [24], if the hardness of reinforcement particles is lower than that of abrasive particles, the particles extract from the matrix or fracture under abrasive particle action. Soft abrasives cannot indent a material surface and adhesion and contact fatigue accompanied by more or less plastic deformation occur as the predominant wear mechanisms [26,27]. Table 3 lists the microhardness of primary $(Cr,Fe)_7C_3$ carbides and eutectic colonies. In this case, the hardness of quartz sands (1000–1100 Hv) is lower than that of the rod-like $(Cr,Fe)_7C_3$ carbides (1300–1350 Hv), but higher than that of eutectic colonies (750–800 Hv). The hardness of blade-like $(Cr,Fe)_7C_3$ carbides is also similar to that of quartz sands. In this study, the relative hardness of quartz sands to eutectic colonies is about 1.25. The quartz sands are harder than the eutectic colonies, so that the quartz sands attack the eutectic colonies easily. The relative hardness of quartz sands to rod-like $(Cr,Fe)_7C_3$ carbides is about 0.75. The quartz sands are soft abrasive particles for primary $(Cr,Fe)_7C_3$ carbides, difficult to indent or plough the primary $(Cr,Fe)_7C_3$ carbides. The relative hardness of quartz sands to blade-like $(Cr,Fe)_7C_3$ carbides is about 0.91. The blade-like $(Cr,Fe)_7C_3$ carbides have less resistance against indentation or plough of quartz sands than the rod-like ones.

The following summarizes carbide content effect on the wear mechanism. Firstly, when the carbide content is 33.8%, abrasives microplough the eutectic colonies and cause carbide fracture. Plastic plows and craters appear in the worn surface. Continuous damage to abrasive particles gradually reveals the harder blade-like $(Cr,Fe)_7C_3$ carbides, owing to their higher hardness. Eventually, the morphology of craters is a polygonal shape. Crater formation is attributed to carbide breakup and pullout. As surface fractions of carbides increase to 61.2%, the plastic plow gradually disappears. The rod-like $(Cr,Fe)_7C_3$ carbides are enough to protect the eutectic colonies. Finally, the wear mechanism fractures or pulls out of carbides when the surface fractions of carbides are 86.1%. The dense $(Cr,Fe)_7C_3$ carbides prevent the eutectic colonies from the plough of quartz sands. However, the quartz sands accumulatively attack the dense $(Cr,Fe)_7C_3$ carbides to cause breakup and pullout. Repeated impingement of quartz sands causes the $(Cr,Fe)_7C_3$ carbides to resist abrasive damage until the carbides break and pullout.

4. Conclusions

The present study uses the FCAW process to form a series of hypereutectic Fe–Cr–C hard claddings. The hard claddings are designed to obtain different carbon contents to investigate the microstructure, wear resistance and wear mechanism of them. The following summarizes the results:

1. The surface fractions of carbides increase with carbon contents increasing. Furthermore, the blade-like carbides occur in the cladding with lower carbon content, but rod-like carbides exist in the one with higher carbon content.
2. Wear resistance not only depends on surface fractions of carbides, but also on cladding hardness and the mean free path of carbides.
3. The rod-like carbides are harder and more resistant than the blade-like ones and the eutectic colonies.
4. More surface fractions of carbides enhance wear resistance and cause the plastic plow to disappear. Crater formation is also attributed to carbide fracture and pullout.

Acknowledgement

The authors are obligated to thank the National Science Council and Ministry of Economic Affairs of Taiwan, ROC for their financial support under projects numbered 98-EC-17-A-08-S1-117, NSC98-2622-E-005-006-C2, and NSC98-2221-E-005-027.

References

[1] C. Fan, M.C. Chen, C.M. Chang, W. Wu, Surf. Coat. Technol. 201 (2006) 908.
[2] L. Lu, H. Soda, A. McLean, Mater. Sci. Eng. A347 (2003) 214.
[3] Y.C. Lin, S.W. Wang, Tribol. Int. 36 (2003) 1.
[4] L.E. Svensson, B. Gretoft, B. Ulander, H.K.D.H. Bhadeshia, J. Mater. Sci. 21 (1986) 1015.
[5] H. Berns, A. Fischer, Mater. Charact. 39 (1997) 499.
[6] A.F. Zhang, J.D. Xing, L. Fang, J.Y. Su, Wear 257 (2004) 198.
[7] H. Berns, Wear 254 (2003) 47.
[8] J.D. Xing, Y.M. Gao, E.Z. Wang, C.G. Bao, Wear 252 (2002) 755.
[9] S. Aso, S. Goto, Y. Komatsu, W. Hartono, Wear 250 (2001) 511.
[10] P.Q. La, Q.J. Xue, W.M. Liu, Wear 249 (2001) 93.
[11] ASM International Handbook Committee, ASM Handbook, tenth ed.ASM International, Materials Park, OH, 1990.
[12] G.V. Raynor, V.G. Rivlin, Phase Equilibria in Iron Ternary Alloys, first ed.The Institute of Metals, USA, 1988.
[13] N.R. Griffing, W.D. Forgeng, G.W. Healy, Trans. TMS-AIME 224 (1962) 148.

[14] R.S. Jackson, J. Iron Steel Inst. 208 (1970) 163.
[15] C.M. Chang, C.M. Lin, C.C. Hsieh, J.H. Chen, W. Wu, J. Alloys Compd. 487 (2009) 83.
[16] S. Chatterjee, T.K. Pal, Wear 255 (2003) 417.
[17] G.L.F. Powell, R.A. Carlson, V. Randle, J. Mater. Sci. 29 (1994) 4889.
[18] S. Atamert, H.K.D.H. Bhadeshia, Mater. Sci. Eng. A130 (1990) 101.
[19] A. Lesko, E. Navera, Mater. Charact. 36 (1996) 349.
[20] C.M. Chang, C.M. Lin, C.C. Hsieh, J.H. Chen, C.M. Fan, W. Wu, Mater. Chem. Phys. 117 (2009) 257.
[21] O.N. Dogan, J.A. Hawk, G. Laird II, Metall. Mater. Trans. A28 (1997) 1315.
[22] R. Colaço, R. Vilar, Wear 255 (2003) 643.
[23] O.N. Dogan, J.A. Hawk, Wear 189 (1995) 136.
[24] K.H. Zum Gahr, Tribol. Int. 31 (1998) 587.
[25] K.H. Zum Gahr, Microstructure and Wear of Materials, Elsevier, USA, 1987.
[26] J. Larsen-Basse, B. Premaratne, International Conference on Wear of Materials, New York, 1983, p. 161.
[27] E. Rabinowicz, International Conference on Wear of Materials, New York, 1983, p. 12.